RSC Advances

PAPER

View Article Online
View Journal | View Issue

Cite this: *RSC Adv.*, 2019, **9**, 1270

Tunable luminescence evolution and energy transfer behavior of $Na_3Sc_2(PO_4)_3:Ce^{3+}/Tb^{3+}/Eu^{3+}$ phosphors†

Yufeng Zhang,[a] Jie Xiong,[a] Dingyi Shen,[a] Wenpeng Xia,[a] Jie Yu,[b] Yanfei Zhang,[c] Jun Yang, *[a] Shanshan Hu,[a] Yuxin Wan,[d] Haili Wen,[d] Hang Ye[d] and Yucan Liu[d]

Received 20th September 2018
Accepted 10th December 2018

DOI: 10.1039/c8ra07827k

rsc.li/rsc-advances

A series of color-tunable emitting $Na_3Sc_2(PO_4)_3:Ce^{3+}/Tb^{3+}/Eu^{3+}$ (NSPO) phosphors were prepared by a combination of hydrothermal synthesis and low temperature calcination. The phase structure, photoluminescence and energy transfer properties of the samples were studied in detail. The tunable colors were obtained by co-doping the Tb^{3+} ions into the NSPO:Ce^{3+} or NSPO:Eu^{3+} phosphors with varying concentrations. Under UV excitation, the energy transfers from Tb^{3+} to Eu^{3+} in the NSPO host occurred mainly *via* a dipole–dipole mechanism, and the critical distances of the ion pairs (R_c) was calculated to be 17.94 Å by the quenching concentration method. And that, the emission colors of the NSPO:Tb^{3+},Eu^{3+} phosphors could be adjusted from green through yellow to red because of the energy transfer from Tb^{3+} to Eu^{3+}. Based on its good photoluminescence properties and abundant emission colors, the NSPO:$Ce^{3+}/Tb^{3+}/Eu^{3+}$ phosphors might be promising as potential candidates for solid-state lighting and display fields.

1 Introduction

When replacing cations in certain hosts, rare earth elements are important activators for modern lighting and display applications, because they have rich emission colors for spectral conversion.[1–5] Recently, rare earth ion-doped inorganic materials have drawn a great deal of attention due to their many applications in optics, magnetics and catalysis.[6–8] In the lighting field, compared with traditional incandescent lighting, white light-emitting diodes (w-LEDs) are favored due to their higher conversion efficiency and more flexible photometric properties.[9–11] Now, the main manufacturing technology of w-LEDs relies on the combination of a blue InGaN chip and a yellow light-emitting phosphor $Y_3Al_5O_{12}:Ce^{3+}$ (YAG). Although this method shows high efficiency, it exhibits a high correlated color and low color rendering index (R_a < 80) because of the lack of a red component.[12] Currently, a new type of w-LEDs assembly which is made by ultraviolet or near ultraviolet excitation single matrix multicolor fluorescent powders is widely used.[13] Therefore, due to the need to increase the efficiency of white light emitting solid state devices, the development of the technique of combining a UV LED chip with tricolor (red, green and blue) phosphors has been proceeding. In this case, recent research has focused on finding converted luminescent phosphors with suitable emission colors, high efficiencies and high chemical stability.

Researchers have studied a variety of inorganic materials, including silicates, aluminates, phosphates, nitrides, molybdates and tungstates. Among them, the rare earth ion-doped phosphate materials have attracted much attention because of their abundance, good chemical stability and low sintering temperature.[14–18] Luminescence of rare earth ions in orthophosphates with the general formula $M^I_3M^{III}(PO_4)_3$ or $M^I_3M^{II}_2(PO_4)_3$ (M^I = Ca, Sr, Ba, Pb, K and Na; M^{III} = La, Y, Gd, Sc, Bi and In) are widely researched.[19–21] As early as the 1980s, scandium phosphate $Na_3Sc_2(PO_4)_3$ (NSPO) was reported and developed as an ion conductor.[22,23] During 2013–2016, Hirohumi studied the luminescent properties of Eu^{2+}-doped NSPO respectively.[24,25] Recently, Huang's group studied the luminescent properties of Eu^{3+} doped NSPO phosphors and NSPO:Ce^{3+},Tb^{3+} phosphors;[26,27] they also reported Dy^{3+} and Eu^{3+} co-doped NSPO phosphors.[28] Among these research reports, the high temperature solid-state reaction method is the most common route to produce orthophosphates. However, it has many disadvantages such as complex experimental conditions, cumbersome procedures and high reaction temperatures (such as 1300 °C).[25–31] Therefore, from the point of view of simplicity and energy saving, there is still an urgent need to develop a simple and mild solution

[a]School of Chemistry and Chemical Engineering, Southwest University, Chongqing 400715, China. E-mail: jyang@swu.edu.cn

[b]Academic Affairs Office, Southwest University, Chongqing 400715, China

[c]School of Mechanical & Automotive Engineering, Qilu University of Technology, Jinan 250061, China

[d]Chongqing Songshuqiao Middle School, Chongqing 401147, China

† Electronic supplementary information (ESI) available. See DOI: 10.1039/c8ra07827k

phase method to produce pure orthophosphate micro/nanocrystals.

Luminescent lanthanide ions can be divided into two categories: 4f–4f and 5d–4f transitions, respectively. Due to the strict ban of 4f–4f transitions, their emission peak widths are very narrow and fixed. For 5d–4f transitions, the 5d orbitals are exposed to the environment and their emission spectra are strongly influenced by the host, such as the strength of the crystal field.[32] We know that the energy transfer process may be affected by the presence of carrier traps or defects in the host lattice. Therefore, it is possible for the tiny dopants with different affinities to change the trap configuration and thus significantly improve the efficiency.[33] It is clear that Tb^{3+} acts as a good sensitizer to increase the luminescence efficiency of Eu^{3+} ions in $Na_3Gd(PO_4)_2$,[34] $CaYAlO_4$,[35] $SrMg_2LaW_2O_{12}$ (ref. 36) and Y_2O_3 (ref. 37) phosphors. Therefore, Tb^{3+} and Eu^{3+} ions can be used as efficient luminescent centers in real devices. Ce^{3+} ions with permissive 5d–4f emission transitions from 300 to 400 nm have been widely studied as efficient activators.[38,39] In addition, Tb^{3+} may also be an important activator with only weak absorption peaks at about 300–400 nm due to the 4f–4f absorption transitions.[40] Therefore, Ce^{3+} ions co-doped in the host can not only increase the emission intensity of Tb^{3+} ions but also cause excitation in the ultraviolet region of 200–400 nm, thereby overcoming the defects of the Ce^{3+} or Tb^{3+} ions doped alone. So far, many Ce^{3+} and Tb^{3+} co-doped materials have been reported including silicates, aluminates, phosphates, fluorides and oxynitrides.[41–44] To the best of our knowledge, the energy transfer of $Tb^{3+} \rightarrow Eu^{3+}$ in NSPO materials by a simple method has little been reported in the previous literature.[24,25,27]

In this work, Tb^{3+}–Eu^{3+} (Ce^{3+}–Tb^{3+}) co-doped NSPO phosphors were firstly synthesized by a combination of hydrothermal method and low temperature calcinations (800 °C). And we obtained tunable emission colors such as red (Eu^{3+}), green (Tb^{3+}), blue-violet (Ce^{3+}), yellow (Tb^{3+}–Eu^{3+}) and so on. The energy transfer mechanisms, the lifetimes, luminescence properties, crystallinity and color tunability of the NSPO:Tb^{3+}–Eu^{3+} phosphors were also investigated. Based on multicolor tunable luminescence, the NSPO:Ce^{3+}/Tb^{3+}/Eu^{3+} phosphors may have potential applications in the field of color displays, fluorescent lamps, solid-state lighting and UV-pumped LEDs.

2 Experimental section

2.1 Materials

The rare earth oxides including Sc_2O_3 (A.R.), CeO_2 (99.99%), Eu_2O_3 (99.99%) and Tb_4O_7 (99.99%) were purchased from Chuandong Chemical Reagents Company (China). The raw materials sodium citrate ($Na_3C_6H_5O_7 \cdot 2H_2O$) (A.R.), sodium phosphate tribasic dodecahydrate ($Na_3PO_4 \cdot 12H_2O$) (A.R.) and hydrogen peroxide (H_2O_2) were purchased from Aladdin (China). All chemicals were used directly without further purification. The $RECl_3$ (RE = Sc, Ce, Eu and Tb) were firstly obtained by dissolving the corresponding rare earth oxides in dilute HCl solution. In addition, it was necessary to add H_2O_2 when dissolving CeO_2 in dilute HCl solution.

2.2 Synthesis

In a typical process of preparing $Na_3Sc_2(PO_4)_3$ host, 2 mmol $Na_3C_6H_5O_7 \cdot 2H_2O$ was added to 30 mL deionized water. After vigorous stirring for 30 min, 2 mmol $ScCl_3$ was added into the above solution for 30 min. Then, it was kept stirring for another 30 min. Subsequently, 2 mmol $Na_3PO_4 \cdot 12H_2O$ was added into the above reaction solution. After additional agitation for 15 min, the obtained mixing solution was transferred into a 50 ml Teflon-lined stainless steel autoclave and maintained at 180 °C for 24 h. When autoclave cooled to room temperature naturally, the obtained samples were collected by centrifugation, washed several times with deionized water and ethanol and then dried at 60 °C for 24 h. Finally, the obtained precipitates were transferred to muffle stove with the temperature at 800 °C for 2 h to get the final products $Na_3Sc_2(PO_4)_3$ (marked as NSPO). A series of NSPO:Ce^{3+}/Tb^{3+}/Eu^{3+} and NSPO:Tb^{3+},Eu^{3+}/Ce^{3+},Tb^{3+} phosphors have been synthesized using the same method above except for different stoichiometric amounts of $RECl_3$ (RE = Sc, Ce, Eu and Tb). Our sample synthesis has good reproducibility, which can also be seen from the XRD, SEM and PL results of the samples in the Results and discussion section.

2.3 Characterization

X-ray power diffraction (XRD) measurements were performed on a Purkinje General Instrument MSALXD3 using Cu Kα radiation (λ = 0.15406 nm). The morphology analysis was carried out on a field emission scanning electron microscopy (FESEM, Hitachi, S-4800). The PL excitation and emission spectra were detected by an F-7000 spectrophotometer (Hitachi, Japan) equipped with a 150 W xenon lamp as excitation source. The decay lifetimes were measured by FLS980 (Edinburgh Instrument).

3 Results and discussion

3.1 Phase, structure and morphology

The crystal structure and phase composition of the samples were studied by X-ray diffraction (XRD). Fig. 1A shows the XRD patterns of pure NSPO (a), NSPO:0.1Ce^{3+} (b), NSPO:0.1Tb^{3+} (c), NSPO:0.1Eu^{3+} (d), NSPO:0.1Tb^{3+},0.1Eu^{3+} (e) and NSPO:0.1Ce^{3+}, 0.01Tb^3 (f), respectively. All diffraction peaks can be attributed to the pure monoclinic NSPO phase, which is consistent with the standard card (JCPDS#44–0567). No other impurities are detected, indicating that the resulting products consist of a microscopic substructure with high crystallinity. The results show that the doped Ln^{3+} ions do not change the phase of the matrix significantly, and the dopant ions have been successfully dissolved in the lattice of NSPO host. It is well known that the chemical properties and ionic radius of the rare earth ions are similar, so we confirm that the Ce^{3+}, Tb^{3+}, Eu^{3+}, Ce^{3+}/Tb^{3+} or Tb^{3+}/Eu^{3+} are well incorporated into the NSPO host lattice. It is worth noting that the characteristic diffraction peak (112) is shifted to a lower diffraction angle. This means that the incorporated ions cause the lattice to expand and the doped rare earth ions have replaced the ions in the body. This further shows that Ce^{3+}, Tb^{3+} and Eu^{3+} are successfully constructed into

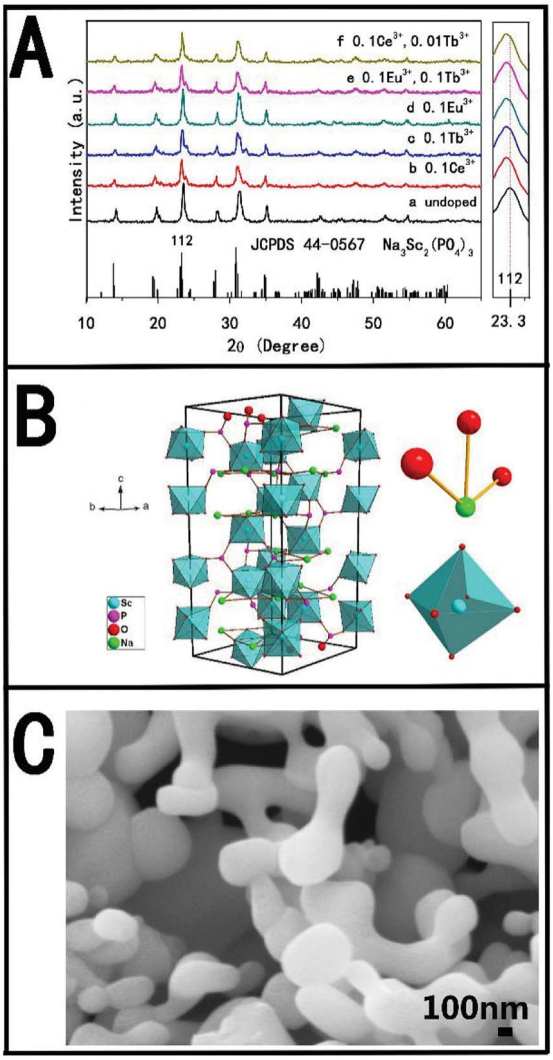

Fig. 1 (A) XRD patterns of pure NSPO (a) and NSPO:Ln^{3+} (b–f); (B) the structure of the NSPO crystals and the sites of Na^+ and Sc^{3+} polyhedrons, respectively; (C) SEM of the prepared NSPO samples.

NSPO host material by doping strategy. Fig. 1B presents the cell structure of the NSPO crystal and the coordination environment of cation Sc^{3+}/Na^+ with O atoms. The detailed structural parameters and crystallographic data for NSPO crystal are listed in Table S1 (ESI†). In the monoclinic NSPO structure, each Sc^{3+} ion is coordinated by its nearest six oxygen atoms to form a regular quadrangular pyramid where Sc^{3+} ion is located in the symcenter. The Na^+ ion is coordinated by eight oxygen atoms. The NSPO compound with lattice constants $a = b = 8.931$ and $c = 22.3267$ crystallizes in the $R\bar{3}c$ space group. The relevant atomic parameter data are listed in Table S2 (ESI†). As shown in Fig. 1C, we found that the NSPO products are relatively uniform nanoparticles with smaller size of 300 nm comparing with the literature reports[26–28] (Fig. S1, ESI†).

3.2 Photoluminescence properties

A series of independently doped NSPO:Ln^{3+} (Ln = Ce/Tb/Eu) and double doped NSPO:Ln^{3+} (Ln = Tb,Eu/Ce,Tb) phosphors were synthesized and their respective luminescence spectra were studied. Eu^{3+} ions are noted activators in various host lattices. Fig. 2a displays the PLE and PL spectra of NSPO:0.1Eu^{3+} phosphors. Monitored at 619 nm, the excitation spectrum includes a weak broad band at 275 nm, which can be attributed to the charge-transfer (CT) band from O^{2-} to Eu^{3+} ions. There are some sharp peaks in the ultraviolet range of 300–400 nm, which can be assigned to the f → f characteristic transition of Eu^{3+} ($^7F_0 \rightarrow {}^5H_5$ at 323 nm, $^7D_0 \rightarrow {}^5D_4$ at 358 nm, $^5D_0 \rightarrow {}^5L_7$ at 380 nm and $^7F_0 \rightarrow {}^5L_6$ at 394 nm).[45] The strongest one is located at near-UV region of 394 nm which indicates that the phosphor is suitable for excitation of UV LED chips. Upon excitation at 394 nm, the PL spectrum includes two emissions peaks at 594 and 619 nm originating from the $^5D_0 \rightarrow {}^7F_1$ and $^5D_0 \rightarrow {}^7F_2$ transitions of Eu^{3+} activator, respectively. We know that the relative intensity of emission is affected obviously by the replaced position of activator Eu^{3+} in host lattice. The $^5D_0 \rightarrow {}^7F_1$ transition corresponding to the magnetic dipole moment is less sensitive to the crystallographic site symmetry of activator Eu^{3+} than the $^5D_0 \rightarrow {}^7F_2$ transition corresponding to the electrical dipole moment transition. Therefore, if Eu^{3+} occupies a high symmetry site, the $^5D_0 \rightarrow {}^7F_1$ emission will be stronger; whereas the $^5D_0 \rightarrow {}^7F_2$ emission dominates the emission spectrum if Eu^{3+} ions locate in a low symmetry site (Fig. 2a).[46,47]

We compared the PL and PLE of the $Na_3Sc_2(PO_4)_3$ doped with Eu^{3+} by both methods (ceramic and hydrothermal) in Fig. S2 (ESI†). Under excitation of 394 nm, the PL spectra of $Na_3Sc_2(PO_4)_3$:Eu^{3+} phosphors by both methods both exhibited four characteristic emission bands with 594(593), 619(621), 654 and 699 nm corresponding to $^5D_0 \rightarrow {}^7F_1$, $^5D_0 \rightarrow {}^7F_2$, $^5D_0 \rightarrow {}^7F_3$ and $^5D_0 \rightarrow {}^7F_4$ transitions, respectively. The emission spectrum of the sample by ceramic method appears to be more refined and has higher luminous intensity at 654 and 699 nm, which can be attributed to higher crystallinity caused by the ceramic method at higher temperature. In the PLE spectra of

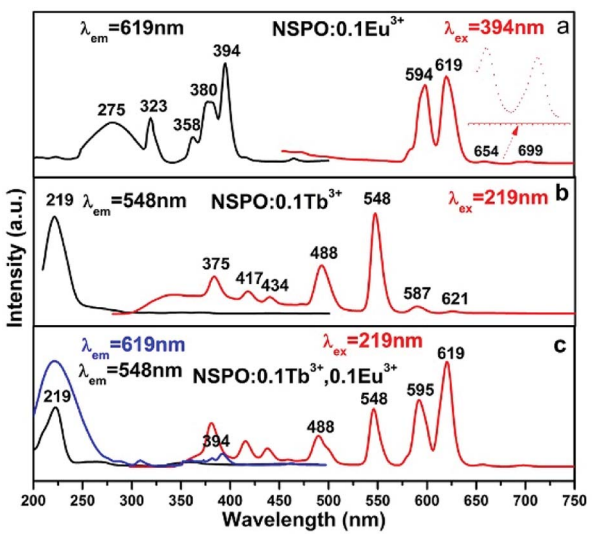

Fig. 2 PL and PLE spectra of the NSPO:0.1Eu^{3+} phosphor (a), NSPO:0.1Tb^{3+} phosphor (b) and NSPO:0.1Tb^{3+},0.1Eu^{3+} phosphor (c), respectively.

$Na_3Sc_2(PO_4)_3$:Eu^{3+} phosphors by both methods, the broad band in the 250–300 nm region was both attributed to the CTB transition from the fully filled 2p orbitals of O^{2-} ions to the partially filled 4f orbitals of Eu^{3+}. Furthermore, these narrow PLE peaks located at around 323(318), 358(364), 380(384) and 394 nm were all attributed to the intra-4f transitions of Eu^{3+} ions from $^7F_0$ level to $^5H_6$, $^5D_4$, $^5L_7$ and $^5L_6$ level, respectively. Compared with Fig. S2A(a),† there was no peak at 297 nm in Fig. S2B(a)† because of the overlap of the CTB band and the $^7F_0 \rightarrow {}^5F_J$ transition of Eu^{3+}. The excitation spectrum of the sample by ceramic method appears to be more refined, which can be also attributed to higher crystallinity caused by the ceramic method at higher temperature.

Fig. 2b shows the PLE and PL spectra of NSPO:0.1Tb^{3+}. We know that Tb^{3+} has a simple 4f configuration energy level structure with low energy state ^7F_J (J = 6, 5, …, 0) and excited states $^5D_{3,4}$. The excitation spectrum (left) at room temperature (RT) is recorded by monitoring with bright green emission at 548 nm, which showed a strong spectral band at 219 nm owing to the $4f^8 \rightarrow 4f^7 5d^1$ transition of the Tb^{3+} ions. Here, we can see several weak peaks in the range of 300–500 nm, which are caused by the spin and orbital forbidden intra-4f transitions (enlarged and shown in Fig. S3†). Excited at the wavelength of 219 nm, the NSPO:0.1Tb^{3+} samples have two emission groups, one is the blue emission caused by the $^5D_3 \rightarrow {}^7F_J$ transitions, and the other is the green emission caused by the $^5D_4 \rightarrow {}^7F_J$ transitions. Four typical transitions from $^5D_4$ level down to ^7F_J levels of $4f^8$ configuration of Tb^{3+} were observed, that is, $^5D_4 \rightarrow {}^7F_6$ at 488 nm, $^5D_4 \rightarrow {}^7F_4$ at 587 nm, $^5D_4 \rightarrow {}^7F_3$ at 621 nm and $^5D_4 \rightarrow {}^7F_5$ at 548 nm (the strongest one). Furthermore, there are three weaker emission peaks at 375 nm, 417 nm and 434 nm, which can be attributed to the $^5D_3 \rightarrow {}^7F_6$, $^5D_3 \rightarrow {}^7F_5$ and $^5D_3 \rightarrow {}^7F_4$ transitions of Tb^{3+}, respectively. The emission spectra illustrate that phosphor NSPO:0.1Tb^{3+} shows an intense green emission. Comparing the excitation band of NSPO:0.1Eu^{3+} with the emission band of NSPO:0.1Tb^{3+} (Fig. 2a and b), a meaningful spectral overlap was observed, which facilitated the transfer energy from Tb^{3+} to Eu^{3+}.

Fig. 2c shows the PLE and PL spectra of the typical NSPO:0.1Tb^{3+},0.1Eu^{3+} sample. The excitation spectra under the detection wavelength of 619 nm and 548 nm (Fig. 2c) are both the same as the excitation spectra of the single doped Tb^{3+} in Fig. 2b (219 nm), indicating that double doped NSPO phosphors can be used as a green and red two-color phosphors in near-UV pumped white LEDs. On the other hand, the emission peaks of the Tb^{3+}–Eu^{3+} co-doped phosphors under 219 nm excitation were observed at 619 nm ($^5D_0$–$^7F_2$) and 548 nm ($^5D_4$–$^7F_5$), which are attributed to the Eu^{3+} and Tb^{3+} ions, respectively. Moreover, 595 nm ($^5D_0$–$^7F_1$) in the orange region of Eu^{3+} as well as 488 nm ($^5D_4$–$^7F_6$) in the blue region of Tb^{3+} can be also observed in the NSPO:0.1Tb^{3+},0.1Eu^{3+} phosphors. From the Fig. 2, we can see that the co-doping of the Tb^{3+} ions have greatly improved the Eu^{3+} emission under same irradiation by comparing the emission spectra of the NSPO:0.10Tb^{3+},0.1Eu^{3+} (Fig. 2c) and NSPO:0.1Eu^{3+} phosphors (Fig. 2a). Most notably, the intensity of the characteristic emitter region of Tb^{3+} is weaker than that of Eu^{3+}, which provides sufficient evidence for effective energy transfer from the donor Tb^{3+} to the receptor Eu^{3+}. Therefore, adjusting the concentrations of the two activators can change the relative intensities of the two emissions by the principle of energy transfer, which is a viable way to get multicolor light emission.

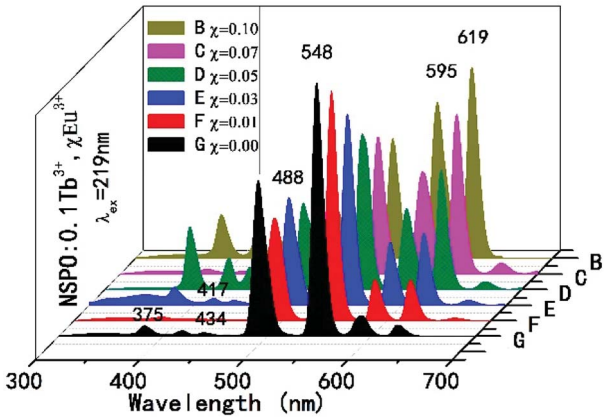

Fig. 3 Emission spectra of the NSPO:0.1Tb^{3+},$x$$Eu^{3+}$ phosphors.

In order to further understand the energy transfer between the Tb^{3+} and Eu^{3+} ions, a series of composition-controlled samples were prepared. Fig. 3 displays the emission spectra of NSPO:0.1Tb^{3+},$x$$Eu^{3+}$ phosphors with x varying from 0 to 0.1. Under excitation at 219 nm UV light, the phosphors show the characteristic emissions of Tb^{3+} as well as sharp emission peaks of Eu^{3+}. Keeping the concentration of Tb^{3+} at 0.1, the emission intensity of Eu^{3+} at 595/619 nm gradually increases with the increase of Eu^{3+} concentration, while the emission intensity of Tb^{3+} at 488/548 nm decreases. Under excitation of characteristic excitation peaks of Tb^{3+} at 219 nm, the changing of Tb^{3+} and Eu^{3+} emission relative intensity in NSPO:0.1Tb^{3+},$x$$Eu^{3+}$ phosphors can further prove the efficient energy transfer from Tb^{3+} to Eu^{3+} ions. In addition, the variations of the Eu^{3+} and Tb^{3+} emission intensity in NSPO:0.1Eu^{3+},$y$$Tb^{3+}$ phosphors is displayed in Fig. S4,† which also reflect the same result of energy transfer from Tb^{3+} to Eu^{3+}.

For more directly observing the changes of relative emission intensity, Fig. 4 presents the variations of Tb^{3+} at 548 nm and Eu^{3+} at 619 nm upon changing the Eu^{3+} content. It is found that the emission intensity of Tb^{3+} ions decreases monotonically with increasing the content of the Eu^{3+} ions; whereas the emission intensity of Eu^{3+} ions as well as the energy transfer efficiency gradually increases. These results further support the generation of effective energy transfer from Tb^{3+} to Eu^{3+} ions. Here, the energy transfer efficiency (η_T) of $Tb^{3+} \rightarrow Eu^{3+}$ in the NSPO host can be estimated using the following formula:[48]

$$\eta_T = 1 - I_S/I_{S0}$$

where I_S and I_{S0} are the luminescence intensities of Tb^{3+} in the presence and absence of Eu^{3+}, respectively. It is clearly discovered that the value of η_T gradually increases with the increase of Eu^{3+}, as shown in Fig. 4 (red line). When x = 0.1, the η_T is as high as 84.72% for NSPO:0.1Tb^{3+},0.1Eu^{3+} phosphors. Generally speaking, energy transfer from sensitizer (Tb^{3+}) to activator

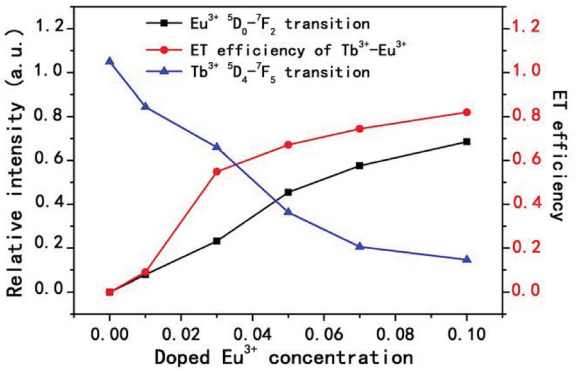

Fig. 4 Relative emission intensities of Eu^{3+} at 619 nm and Tb^{3+} at 548 nm, and the ET efficiency of $Tb^{3+} \rightarrow Eu^{3+}$ in NSPO:0.1Tb^{3+},xEu^{3+} phosphors ($x = 0$–0.1).

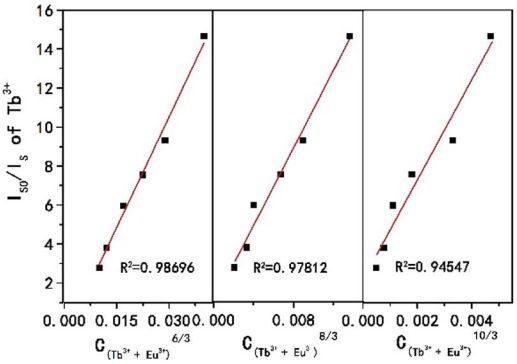

Fig. 5 Dependence of I_{S0}/I_S of Tb^{3+} on $C_{(Tb^{3+}+Eu^{3+})}^{6/3}$, $C_{(Tb^{3+}+Eu^{3+})}^{8/3}$ and $C_{(Tb^{3+}+Eu^{3+})}^{10/3}$, respectively.

(Eu^{3+}) can be achieved through the exchange interaction or electric multipolar interaction.[49] If the energy transfer is caused by the exchange interaction, the critical distance between the sensitizer and the activator should be less than 3–4 Å. In contrast, electrical multipolar interaction may dominate.[50] The critical distance R_c of energy transfer was calculated by using the concentration quenching method, where the critical distance R_c can be calculated by the following formula presented by Blasse:[51]

$$R_c \approx 2\left[\frac{3V}{4\pi x_c N}\right]^{1/3}$$

Here V is the unit cell volume, x_c is the critical concentration and N refers to the number of formula units per unit cell. For the NSPO host, $V = 1542.20$ Å^3, $x_c = 0.085$ and $N = 6$. Based on the above formula, the critical distance for energy transfer is estimated to be about 17.94 Å. The value is longer than 3–4 Å, indicating that the energy transfer mechanism is controlled by electrical multipolar interaction in this system. We have further discussed the energy transfer mechanism for electrical multipolar interaction, which can be determined using the following relationship:[52,53]

$$\eta_0/\eta \propto C^{n/3}$$

Here η_0 and η are the luminescence quantum efficiencies of Tb^{3+} in the absence and presence of Eu^{3+}, respectively; and the values of η_0/η can be approximately calculated by the ratio of related luminescence intensities (I_{S0}/I_S); C is the concentration of the sum of Tb^{3+} and Eu^{3+}; and $n = 6$, 8 and 10 correspond to dipole–dipole, dipole–quadrupole and quadrupole–quadrupole interaction, respectively. The relationships between I_{S0}/I_S and $C_{(Tb^{3+}+Eu^{3+})}^{n/3}$ are illustrated in Fig. 5 for NSPO:0.1Tb^{3+},xEu^{3+} phosphors. The best linear behavior was observed when $n = 6$ based on the values of the fitting parameters R^2, implying that the $Tb^{3+} \rightarrow Eu^{3+}$ energy transfer occurs by the dipole–dipole interaction.

To further validate the energy transfer phenomenon, the decay curves of Tb^{3+} emission of NSPO:0.1Tb^{3+},xEu^{3+} ($x = 0$, 0.01, 0.05, 0.10) phosphors are shown in Fig. 6. We can see that all decay curves can be well fitted by the first order exponential decay method using the formula:[54,55]

$$I_{(t)} = I_0 \exp(-t/\tau)$$

where τ is the $1/e$ lifetime of Tb^{3+}. According to the formula, the decay times were calculated to be 3.36, 2.84, 1.97 and 0.86 ms for NSPO:0.1Tb^{3+},xEu^{3+} with $x = 0$, 0.01, 0.05 and 0.10, respectively. It is easy to find that the decay lifetime of the Tb^{3+} ions decreases monotonically with the Eu^{3+} concentration increasing, which further confirms the existence of energy transfer from Tb^{3+} to Eu^{3+} ions.[51] Based on the principle of energy transfer, a coordinated emission of colors can be achieved by varying the proportion of doping content. A representative CIE chromaticity diagram and coordinates of NSPO:0.1Tb^{3+},xEu^{3+} ($x = 0$–0.1) phosphors are calculated from the relevant PL spectra (Fig. 3), as shown in Fig. 7. With the increase of Eu^{3+} concentration, the CIE coordinates range from (0.2865, 0.4982) through (0.3657, 0.4516) to (0.5693, 0.2976); and the emission colors change from green through yellow to red, accordingly. Thus, we make sure that tunable luminescence can be achieved in the new NSPO:0.10Tb^{3+},xEu^{3+} phosphors based on energy transfer.

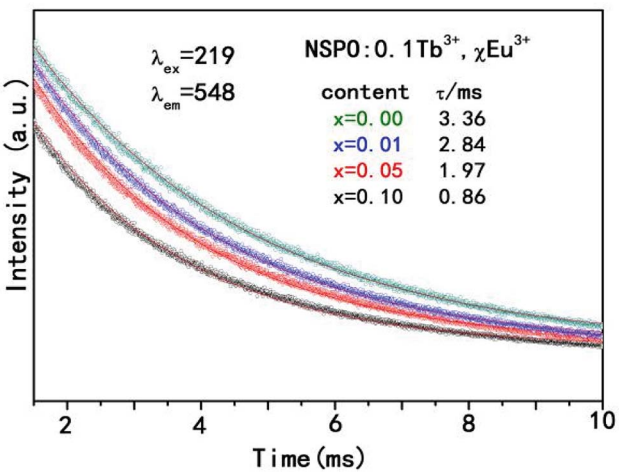

Fig. 6 Decay curves of Tb^{3+} in NSPO:0.1Tb^{3+},xEu^{3+} ($x = 0$, 0.01, 0.05, 0.10) phosphors.

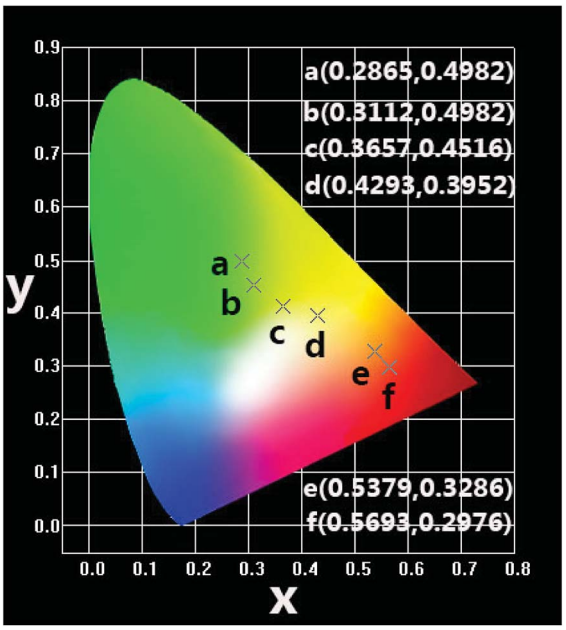

Fig. 7 CIE chromaticity coordinates of NSPO:0.1Tb^{3+},xEu^{3+} (x = 0–0.1) phosphors under 219 nm excitation.

Fig. 8 displays the PLE and PL spectra of Ce^{3+} or Tb^{3+} solely doped and Ce^{3+}/Tb^{3+} co-activated NSPO phosphors. Ce^{3+} ions have been doped into the host as activator, and the luminescent properties have been explored. As shown in Fig. 8a, the excitation spectrum monitored at 367 nm for NSPO:0.1Ce^{3+} phosphors exhibit a broad band centered at 278 nm, which corresponds to the transition from the 4f state of Ce^{3+} ions to the excited Ce^{3+} ions 5d state. Under the irradiation at 278 nm, the phosphors can emit intense blue-violet light with a peak wavelength at 367 nm which can be attributed to the lowest Ce^{3+} 5d excited state to the ground state $^2F_{5/2}$ in the Ce^{3+} 4f configuration. Generally, with a low doping concentration of Tb^{3+} in the host matrix, the character emission of Tb^{3+} is rather weak. Fig. 8b displays the excitation and emission spectra of NSPO:0.01Tb^{3+}. The excitation spectrum shows a strong broad absorption band (219 nm) with shoulders at 257/273 nm arising from an allowed $4f^8$–$4f^7$5d transition and some weak narrow absorption peaks from 300 to 500 nm due to intra-(4f) transitions of Tb^{3+}. The shoulders may originate from the forbidden component of the $4f^8$–$4f^7$5d transition.[56] Based on the above PL spectrum of the Ce^{3+} single-doped sample and the PLE spectrum of the Tb^{3+} single-doped sample (Fig. 8a and b), the spectral overlap between the broad emission band of Ce^{3+} and the Tb^{3+} excitation within the spectral range of 300–400 nm. Thus, it is expected that a resonance-type ET from Ce^{3+} to Tb^{3+} may occur in the NSPO host. As shown in Fig. 8c, the PLE and PL spectra of NSPO:0.1Ce^{3+},0.01Tb^{3+} phosphors were studied. When monitored at 548 nm of Tb^{3+}, the excitation spectrum consists of an excitation band (219 nm) of Tb^{3+} ions assigned to f-d transitions and a strongest excitation band (278 nm) of Ce^{3+} ions, indicating the possible energy transfer from Ce^{3+} to Tb^{3+} ions. Moreover, when excited at 278 nm, the PL spectra show not only the broad emission peak in the blue-violet region from the electric-dipole-allowed 4f–5d transitions of Ce^{3+} (367 nm), but also the strong emission of Tb^{3+}at 488 nm and 548 nm ($^5D_4$–$^7F_{J=6,5}$), which also provides another evidence for the energy transfer from Ce^{3+} to Tb^{3+}. To know the energy transfer process, a series of samples with different concentrations of Ce^{3+} were prepared. Fig. S5† shows the emission spectrum of the NSPO:0.01Tb^{3+},yCe^{3+}(y = 0, 0.05, and 0.10) phosphors upon an excitation wavelength of 278 nm. When the Tb^{3+} doping concentration is fixed, the Tb^{3+} emission intensity increases monotonously and the Ce^{3+} emission intensity decreases as the Ce^{3+} ion concentration increases. This should be due to the enhancement of energy transfer from Ce^{3+} ions to Tb^{3+} ions.

The decay curves and lifetime of Ce^{3+} in NSPO:0.1Ce^{3+},yTb^{3+} (y = 0, 0.01) are showed in Fig. 9 According to the decay behavior of Ce^{3+}, their corresponding luminescence decay curve can be best fitted to the typical second-order decay method by the following equation:[57]

$$I_{(t)} = A_1 \exp(-t/\tau_1) + A_2 \exp(-t/\tau_2)$$

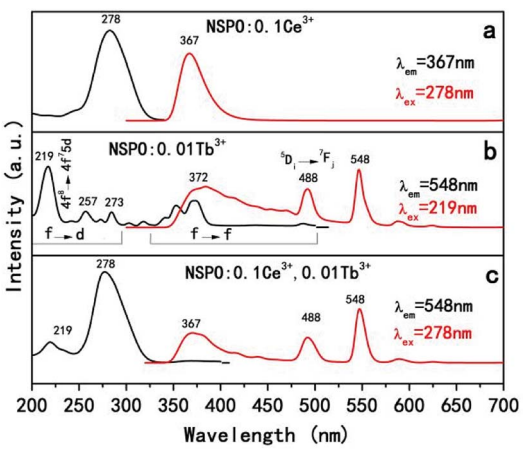

Fig. 8 PLE and PL spectra of NSPO:0.1Ce^{3+} (a), NSPO:0.01Tb^{3+} (b) and NSPO:0.1Ce^{3+},0.01Tb^{3+} (c), respectively.

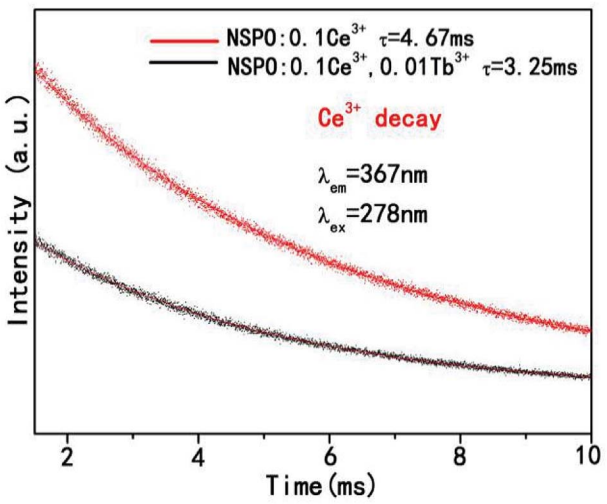

Fig. 9 The decay curves and lifetime of Ce^{3+} in NSPO:0.1Ce^{3+},yTb^{3+} (y = 0, 0.01).

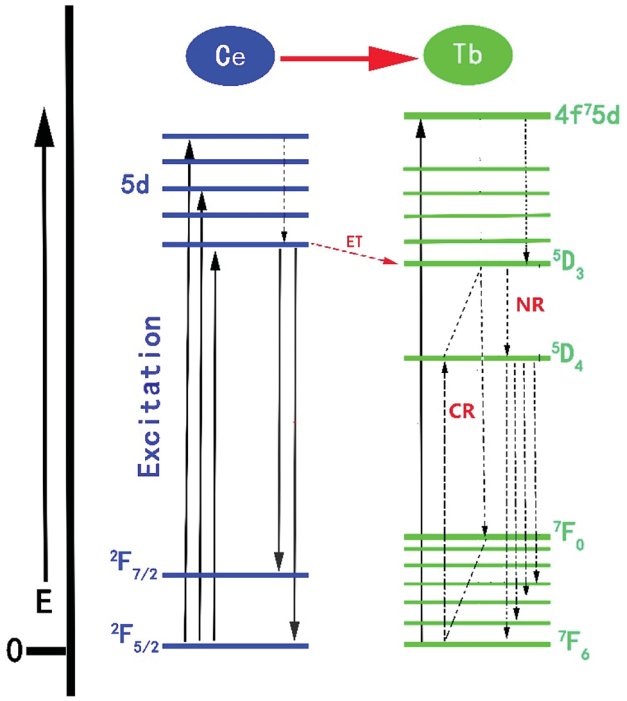

Fig. 10 Energy level model for the ET processes of $Ce^{3+} \rightarrow Tb^{3+}$ in NSPO host.

Here I is the luminescence intensity at time t; A_1 and A_2 are two constants which are related with the initial intensity; τ_1 and τ_2 are rapid and slow times for the exponential components, respectively. The average lifetime (τ) can be calculated using the following equation:

$$\tau = (A_1\tau_1^2 + A_2\tau_2^2)^2/(A_1\tau_1 + A_2\tau_2)$$

The lifetime of Ce^{3+} is 4.67 ms when doped only with Ce^{3+} ions in NSPO phosphors. However, the lifetime of Ce^{3+} decreases to 3.25 ms with the introduction of Tb^{3+}, demonstrating the energy transfer from Ce^{3+} to Tb^{3+} by non-radiative processes.[58]

The proposed $Ce^{3+} \rightarrow Tb^{3+}$ ET process in the NSPO host is shown in Fig. 10. Firstly, Ce^{3+} ions can effectively absorb UV light from the ground state ($^2F_{5/2}$) to the excited state (5d energy levels) by UV irradiation. Secondly, these electrons relax to the lowest vibrational level of the excited state to release excess energy into the surrounding environment and then either return to the ground states to produce the Ce^{3+} emissions; or efficiently transfers the energy to the $^5D_3$ level of Tb^{3+}, followed by non-radiative relaxation to $^5D_4$ level ($^5D_3 + {}^7F_6 = {}^5D_4 + {}^7F_0$) due to the same energy difference between $^5D_3 \rightarrow {}^5D_4$ and $^7F_0 \rightarrow {}^7F_6$ in Tb^{3+} ions.[56,59] Finally, as a result of the electrons moving from the $^5D_4$ excited state to the ^7F_J (J = 3, 4, 5, 6) ground state, the green light is obtained.

4 Conclusions

In summary, we have successfully synthesized a series of color tunable NSPO:Ce^{3+}/Eu^{3+}/Tb^{3+} phosphors by a combination of hydrothermal method and low temperature calcinations (800 °C). The obtained NSPO:Ce^{3+}/Eu^{3+}/Tb^{3+} phosphors were relatively uniform nanoparticles with size of 300 nm. The energy transfer of Tb^{3+}/Eu^{3+} co-doping as well as their tunable multi-color luminescence in $Na_3Sc_2(PO_4)_3$ host lattices were realized. Due to energy transfer of $Tb^{3+} \rightarrow Eu^{3+}$, the emission colors of the resulting phosphor can be changed from green (0.2865, 0.4982) to red (0.5693, 0.2976) through yellow (0.3657, 0.4516) by adjusting the concentration of Eu^{3+}. The obtained NSPO:Ce^{3+}/Eu^{3+}/Tb^{3+} phosphors can be promising as a potential candidate for the applications for solid-state lighting and display fields.

Conflicts of interest

There are no conflicts to declare.

Acknowledgements

This project is financially supported by the Fundamental Research Funds for the Central Universities (XDJK2016C147 and XDJK2018C050) and the National Natural Science Foundation of China (51302229).

Notes and references

1 P. Pust, V. Weiler, C. Hecht, A. Tucks, S. A. Wochnik, K. A. Henss, D. Wiechert, C. Scheu, J. P. Schmidt and W. Schnick, *Nat. Mater.*, 2014, **13**, 891–896.
2 A. A. Setlur, E. V. Radkov, C. S. Henderson, J. H. Her, A. M. Srivastava, N. Karkada, M. S. Kishore, N. P. Kumar, D. Aesram, A. Deshpande, B. L. Kolodin, S. Grigorov and U. Happek, *Chem. Mater.*, 2010, **22**, 4076–4082.
3 K. A. Denault, J. Brgoch, M. W. Gaultois, A. Mikhailovsky, R. Petry, H. Winkler, S. P. DenBaars and R. Seshadri, *Chem. Mater.*, 2014, **26**, 2275–2282.
4 Z. Ci, Q. Sun, S. Qin, M. Sun, X. Jiang, X. Zhang and Y. Wang, *Phys. Chem. Chem. Phys.*, 2014, **16**, 11597–11602.
5 X. Li, F. Liu, J. Y. Howe, J. Zhang, X. J. Wang, Z. Gu, C. Sun, R. S. Meltzer and Z. Pan, *Light: Sci. Appl.*, 2013, **2**, 3250–3257.
6 Y. Q. Li, A. C. A. Delsing, G. D. With and H. T. Hintzen, *Chem. Mater.*, 2005, **17**, 3242–3248.
7 K. Hanaoka, K. Kikuchi, T. Terai, T. Komatsu and T. Nagano, *Chemistry*, 2008, **14**, 987–995.
8 C. H. Liang, F. B. Li, C. S. Liu, J. Lu and X. G. Wang, *Dyes Pigm.*, 2008, **76**, 477–488.
9 H. A. Höppe, *Angew. Chem., Int. Ed.*, 2009, **48**, 3572–3582.
10 E. F. Schubert and J. K. Kim, *Science*, 2005, **308**, 1274–1278.
11 T. Justel, H. Nikol and C. Ronda, *Angew. Chem.*, 1998, **37**, 3084–3103.
12 W. Y. Tian, K. X. Song, F. F. Zhang, P. Zheng, J. X. Deng, J. Jiang, *et al.*, *J. Alloys Compd.*, 2015, **638**, 249–253.
13 Z. G. Xia, H. Y. Du, J. Y. Sun, D. M. Chen and X. F. Wang, *Mater. Chem. Phys.*, 2010, **119**, 7–10.
14 J. K. Sheu, S. J. Chang, C. Kuo, Y. K. Su, L. Wu, Y. Lin, W. Lai, J. Tsai, G.-C. Chi and R. Wu, *IEEE Photonics Technol. Lett.*, 2003, **15**, 18–20.

15 T. S. Chan, R. S. Liu and I. Baginskiy, *Chem. Mater.*, 2008, **20**, 1215–1217.
16 N. Guo, W. Lü, Y. Jia, W. Lv, Q. Zhao and H. You, *ChemPhysChem*, 2013, **14**, 192–197.
17 D. Geng, M. Shang, Y. Zhang, H. Lian and J. Lin, *Inorg. Chem.*, 2013, **52**, 13708–13718.
18 W. Wu and Z. Xia, *RSC Adv.*, 2013, **3**, 6051–6057.
19 C. C. Lin, C. C. Shen and R. S. Liu, *Chem.–Eur. J.*, 2013, **19**, 15358–15365.
20 H. B. Liang, Y. Tao, J. H. Xu, H. He, H. Wu and W. X. Chen, *J. Solid State Chem.*, 2004, **117**, 901–908.
21 Z. J. Wang, S. Q. Lou and P. L. Li, *J. Alloys Compd.*, 2014, **586**, 536–541.
22 V. V. Tkachev, V. I. Ponomarev and L. O. Atovmyan, *Zhurnal Strukturnoj Khimii*, 1984, **25**, 128–134.
23 B. I. Lazoryak, V. B. Kalinin, S. Y. Stefanovich and V. A. Efremov, *Dokl. Akad. Nauk SSSR*, 1980, **250**, 861–864.
24 N. Guo, Y. H. Zheng, Y. C. Jia, H. Qiao and H. P. You, *J. Phys. Chem. C*, 2012, **116**, 1329–1334.
25 K. Hirohumi, Master thesis, Niigata University, 2013.
26 H. Guo, X. Y. Huang and Y. J. Zeng, *J. Alloys Compd.*, 2018, **741**, 300–306.
27 H. Guo, B. Devakumar, B. Li and X. Y. Huang, *Dyes Pigm.*, 2018, **151**, 81–88.
28 R. Vijayakumar, H. Guo and X. Y. Huang, *Dyes Pigm.*, 2018, **156**, 8–16.
29 X. C. Wang, Z. Y. Zhao, Q. S. Wu, C. Wang, Q. Wang, Y. Y. Li and Y. H. Wamg, *J. Mater. Chem. C*, 2016, **4**, 8795–8801.
30 Y. S. Liu, D. T. Tu, H. M. Zhu and X. Y. Chen, *Chem. Soc. Rev.*, 2013, **42**, 6924–6958.
31 X. Teng, Y. H. Zhu, W. Wei, S. C. Wang, J. F. Huang, R. Naccache, W. B. Hu, A. L. Y. Tok, Y. Han, Q. C. Zhang, Q. Y. Fan, W. Huang, J. A. J. Capobianco and L. Huang, *J. Am. Chem. Soc.*, 2012, **134**, 8340–8343.
32 Y. J. Ding, X. Teng, H. Zhu, L. L. Wang, W. B. Pei, J. J. Zhu, L. Huang and W. Huang, *Nanoscale*, 2013, **5**, 11928–11932.
33 H. Y. Jiao and Y. H. Wang, *J. Electrochem. Soc.*, 2009, **156**, 117–120.
34 H. Yamamoto and K. Urade, *J. Electrochem. Soc.*, 1982, **129**, 2069–2074.
35 D. Wang, Y. Wang and J. W. He, *Mater. Res. Bull.*, 2012, **47**, 142–145.
36 D. Q. Geng, G. G. Li, M. M. Shang, C. Peng, Y. Zhang, Z. Y. Cheng and J. Lin, *Dalton Trans.*, 2012, **41**, 3078–3086.
37 K. Pavani, J. Suresh Kumar and L. Rama Moorthy, *J. Alloys Compd.*, 2014, **586**, 722–729.
38 M. Back, M. Boffelli, A. Massari, R. Marin, F. Enrichi and P. Riello, *J. Nanopart. Res.*, 2013, **15**, 1753–1758.
39 N. Guo, Y. H. Song, H. P. You, G. Jia, M. Yang, K. Liu, *et al.*, *Eur. J. Inorg. Chem.*, 2010, **29**, 4636–4642.
40 W. P. Chen, H. B. Liang, B. Han, J. P. Zhong and Q. Su, *J. Phys. Chem. C*, 2009, **113**, 17194–17199.
41 J. Ding, Q. Zhang, J. Cheng and X. Liu, *J. Alloys Compd.*, 2010, **495**, 205–208.
42 Z. G. Xia and R. S. Liu, *J. Phys. Chem. C*, 2012, **116**, 15604–15609.
43 L. E. Muresan, Y. Karabulut, A. I. Cadis, I. Perhaita, A. Canimoglu and J. Garcia Guinea, *J. Alloys Compd.*, 2016, **658**, 356–366.
44 Q. H. Zhang, H. Y. Ni, L. L. Wang and F. M. Xiao, *Ceram. Int.*, 2016, **42**, 6115–6120.
45 Z. F. Yang, Y. H. Hu, L. Chen, X. J. Wang and G. F. Ju, *Mater. Sci. Eng,. B: Solid State. Mater. Adv. Technol.*, 2015, **193**, 27–31.
46 L. Macalik, P. E. Tomaszewski, R. Lisiecki and J. Hanuza, *J. Solid State Chem.*, 2008, **181**, 2591–2600.
47 Z. X. Tao, T. Tsuboi, Y. L. Huang, W. Huang, P. Q. Cai and H. J. Seo, *Inorg. Chem.*, 2014, **53**, 4161–4168.
48 S. Y. Xin, Y. H. Wang, G. Zhu, X. Ding, W. Y. Geng and Q. Wang, *Dalton Trans.*, 2015, **44**, 16099–16106.
49 P. I. Paulose, G. Jose, V. Thomas, N. V. Unnikrishnan and M. K. R. Warrier, *J. Phys. Chem. Solids*, 2003, **64**, 841–846.
50 R. Reisfeld, E. Greenberg, R. Velapoldi and B. Barnett, *J. Chem. Phys.*, 1972, **56**, 1698–1705.
51 B. M. Antipeuko, I. M. Bataev, V. L. Ermolaev, E. I. Lyubimov and T. A. Privalova, *Opt. Spectrosc.*, 1970, **29**, 177–184.
52 G. Blasse, *J. Solid State Chem.*, 1986, **62**, 207–211.
53 H. Jiao, F. Liao, S. Tian and X. J. Jing, *J. Electrochem. Soc.*, 2003, **150**, 220.
54 D. L. Dexter and J. A. Schulman, *J. Chem. Phys.*, 1954, **22**, 1063–1070.
55 Z. G. Xia, J. Q. Zhuang, A. Meijerink and X. P. Jing, *Dalton Trans.*, 2013, **42**, 6327–6336.
56 J. Hao, S. A. Studenikin and M. Cocivera, *J. Appl. Phys.*, 2001, **90**, 5064–5069.
57 H. L. Li, Z. L. Wang, S. J. Xu and J. H. Hao, *J. Electrochem. Soc.*, 2009, **156**, 112–116.
58 J. Y. Sun, X. Y. Zhang, Z. G. Xia and H. Y. Du, *Mater. Res. Bull.*, 2011, **46**, 2179–2182.
59 D. W. Wen and X. J. Shi, *Dalton Trans.*, 2013, **42**, 16621–16629.